Coupled approach VIM-BEM for efficient modeling of ECT signal due to narrow cracks and volumetric flaws in planar layered media

Roberto Miorelli, Christophe Reboud, Theodoros Theodoulidis, John Martinos, Nikolaos Poulakis, Dominique Lesselier

Coupled approach VIM–BEM for efficient modeling of ECT signal due to narrow cracks and volumetric flaws in planar layered media

Roberto Miorelli[a,*], Christophe Reboud[a], Theodoros Theodoulidis[b], John Martinos[b], Nikolaos Poulakis[c], Dominique Lesselier[d]

[a]Département Imagerie Simulation pour le Contrôle, CEA, LIST, Gif-sur-Yvette 91191, France
[b]Department of Mechanical Engineering, University of Western Macedonia, Kozani 50100, Greece
[c]Department of Electrical Engineering, Technological Educational Institute of Western Macedonia, Koila 50100, Greece
[d]Département de Recherche en Electromagnétisme, Laboratoire des Signaux et Systèmes UMR8506, CNRS-SUPELEC-Université Paris Sud 11, 3 rue Joliot-Curie, Gif-sur-Yvette 91192, France

Rapid and accurate modeling of Eddy Current Testing (ECT) signal is required in many industrial areas. For example, crack detection via ECT is widely employed in aeronautics and aerospace industry to inspect riveted planar multilayered structures. In these structures, small narrow cracks (e.g. micro-cracks) may initiate at the edge of rivet holes (which can be considered as large volumetric flaws) and propagate through the PMS. This paper proposes a new and efficient model, based on a coupled approach between Volume Integral Method (VIM) and Boundary Element Method (BEM), simulating ECT probe signals due to the presence of both narrow cracks located near volumetric flaws within a given PMS. Simulation results are compared with experimental and simulated signals obtained with a numerical code. The performance of the method, in terms of accuracy and computational time, is discussed and the perspectives opened are presented.

1. Introduction

Eddy Current Testing (ECT) is a standard non-destructive inspection method, which is very popular in industry because of its high sensitivity, repeatability and its – usually – low cost in comparison to other techniques. In the process of developing sensors and inspection procedures, the use of simulation tools reduces the number of costly and time consuming hardware experiments and allows an in-depth performance analysis. For these reasons, fast numerical tools are actively developed and widely used in support of electromagnetic nondestructive testing.

In two recent articles [1,2] an efficient model, based on Boundary Element Method (BEM), has been proposed to address in large set of inspection configurations, consisting in the detection with ECT of multiple narrow cracks affecting a planar multi-layered structure. The BEM developed is based on analytical calculations of the spatial-domain Dyadic Green Function (DGF), describing, in general, the electric field emitted in the planarly layered media by an electric dipole source embedded within the same structure.

This spatial operator has been obtained from the spectral-domain DGF, which has been described via vector wave functions approach in [3]. Generalized transmission and reflection coefficients have been used to determine, in a general and convenient way, layers interactions inside the layered structure [4]. By expressing the spectral-domain DGF with a Sommerfeld Integrals (SIs) formalism, closed forms have been obtained using the Discrete Complex Image Method (DCIM) [5] and the Generalized Pencil of Function (GPOF) [6]. Finally, the expression of the spatial-domain DGF has been analytically derived from the closed-form SIs.

ECT simulation with the BEM approach consists in approximating the perturbation of eddy current, induced in the planar stratified half-space by the ECT probe, due to the presence of a narrow crack as the effect of a fictitious dipole distribution located in the flaw volume and oriented toward the direction of its opening. This approximation is valid for a large range of configurations involving cracks with zero and non-zero – but small – openings [7,8,11]. When considering volumetric flaws, the BEM does not address properly the corresponding eddy current perturbation. For such flaws, the classical Volume Integral Method (VIM) [9], describing the field perturbation as the effects of a 3D dipole distribution, is very efficient in terms of both accuracy and

* Corresponding author. Tel.: +33 169085057; fax: +33 169087597.
E-mail addresses: roberto.miorelli@cea.fr (R. Miorelli), christophe.reboud@cea.fr (C. Reboud), theodoul@uowm.gr (T. Theodoulidis), ioannismartinos@gmail.com (J. Martinos), poulakis@teikoz.gr (N. Poulakis), dominique.lesselier@lss.supelec.fr (D. Lesselier).

computation time. However, in the case of narrow flaws, VIM loses its accuracy due to numerical problems. These two approaches are thus very complementary.

This paper proposes a coupled approach between VIM and BEM, called hereafter VIM–BEM, in order to address ECT configurations involving, at the same time, narrow cracks and volumetric flaws. The aim of VIM–BEM is to mitigate the drawbacks of a pure VIM modeling, when narrow cracks are present, and overcome the BEM model limitations in the presence of volumetric flaws. To the authors' knowledge, such a coupled approach has not been developed before, at least in the framework of ECT signal modeling. Even if this work is not focused on a particular kind of ECT application, problems and validations proposed in this paper are close to the aeronautic and aerospace domains, where this problematic situation is often encountered [10,12]. Validation results with respect to laboratory-controlled experiments [13] and numerical code will be presented.

2. Overview of integral equation-based modeling applied to ECT simulation

An overview of both VIM and BEM is given first, as a comprehensive introduction to the description of the coupled VIM–BEM approach. In Fig. 1, a typical application case of interest is depicted. A single coil inspects a riveted structure with two narrow corner cracks departing radially from the rivet hole, the rivet itself being removed. In this paper, the unflawed piece consists in a linear, isotropic and non-magnetic ($\mu=\mu_0$ is the permeability of air) planar stratified medium. Moreover, we assume to work at a given angular frequency ω and with the time-harmonic dependence $e^{-i\omega t}$, which will be omitted in our notation.

2.1. Outline of VIM and BEM models

Both methods use the reciprocity theorem [14] in order to derive the simulated ECT signal. In the case of a single coil inspecting a flawed material, one can show that the variation of coil impedance ΔZ can be expressed for each coil position as

$$\Delta Z=\frac{1}{I^2}\sum_{s=1}^{S}\int_{\Omega_s}\frac{1}{\sigma_s}\mathbf{J}_s^{inc}(\mathbf{r})\cdot\mathbf{p}_s(\mathbf{r})\,d\mathbf{r},\quad \mathbf{r}\in\Omega_s,\quad s\in[1,\ldots,S]. \tag{1}$$

where Ω_s is the volume of the sth flaw present in the piece. $\mathbf{J}_s^{inc}$ is the incident current density induced by the coil in region Ω_s without flaw and $\mathbf{p}_s$ is a fictitious dipole density associated to the flawed region Ω_s, such that its effect, in terms of electric field, corresponds to the difference between the flawed and the unflawed cases. I is the coil driven current and σ_s is the conductivity of the layer where the sth flaw and the associated dipole density $\mathbf{p}_s$ lay. In VIM, $\mathbf{J}_s^{inc}$ and $\mathbf{p}_s$ are vector quantities, whereas in BEM $\mathbf{p}_s$ is assumed to be oriented toward the crack opening, so that it is reduced to a scalar quantity. Distributions $\mathbf{J}_s^{inc}$ are solution of preliminary calculations, consisting in a field computation in the planar structure without rivet hole and without flaws, which are fast and accurately carried out using semi-analytical techniques [15]. The unknowns of the problem are the fictitious dipole densities $\mathbf{p}_s$, which are solutions of a system of S integral equations. These equations are either Fredholm equations of the second kind for VIM [9] as

$$\mathbf{J}_o^{inc}(\mathbf{r})=\mathbf{p}_o(\mathbf{r})-\sum_{s=1}^{S}f_o(\mathbf{r})k_o^2\int_{\Omega_s}\underline{\mathbf{G}}_{os}(\mathbf{r},\mathbf{r}')\mathbf{p}_s(\mathbf{r}')\,d\mathbf{r}',\quad \mathbf{r}'\in\Omega_s,\quad \mathbf{r}\in\Omega_o,\quad o\in[1,\ldots,S], \tag{2}$$

or Fredholm equations of the first kind for BEM [1,2] as

$$\mathbf{n}_o\cdot\mathbf{J}_o^{inc}(\mathbf{r})=-\sum_{s=1}^{S}f_o(\mathbf{r})k_o^2\int_{\Omega_s}\mathrm{G}_{os}^{n_on_s}(\mathbf{r},\mathbf{r}')\mathrm{p}_s(\mathbf{r}')\,d\mathbf{r}',\quad \mathbf{r}'\in\Omega_s,\quad \mathbf{r}\in\Omega_o,\quad o\in[1,\ldots,S]. \tag{3}$$

In these equations, subscripts s and o are employed to denote the quantities associated to the source and the observation, respectively. If only one crack occupies the planar layered structure, then $s=o$. The system (2) is made of S vector integral equations, whereas in system (3), the integral equations are reduced to S scalar equations by projection onto directions $\mathbf{n}_o$ of the flaws openings. The contrast function $f_o(\mathbf{r})$ is defined as $f_o(\mathbf{r})=[\sigma(\mathbf{r})-\sigma_o]/\sigma_o$ where $\sigma(\mathbf{r})$ and σ_o are the flaw and the hosting layer conductivity, respectively. The wave number $k_o=\sqrt{i\omega\mu_0\sigma_o}$ is associated to the layer hosting the oth flaw.

In (2) the quantity $\mathbf{p}_o(\mathbf{r})$ represents the total current density within the observation zone. Moreover, within (2) the electric–electric dyadic Green function $\underline{\mathbf{G}}_{os}(\mathbf{r},\mathbf{r}')$, is used to describe the electric field due to a vector source located in $\mathbf{r}'$ at a point located in $\mathbf{r}$. Its component $G_{os}^{n_on_s}(\mathbf{r},\mathbf{r}')$ in (3) describes the effect of an $\mathbf{n}_s-$oriented dipole placed in $\mathbf{r}'$ onto the $\mathbf{n}_o-$oriented component of the electric field at a given observation point $\mathbf{r}$.

In order to solve (2) and (3), flawed regions are uniformly meshed in parallelepiped cells. After the application of the Method of Moments (MoM) [16] the following two matrix systems are obtained for VIM and BEM, respectively.

$$[\mathbf{J}_o^{inc}]=[\mathbf{p}_o]-[\underline{\mathbf{G}}_{os}][\mathbf{p}_s], \tag{4}$$

and

$$[\mathbf{J}_o^{inc}]=-[\mathrm{G}_{os}^{n_on_s}][\mathrm{p}_s]. \tag{5}$$

One can readily notice that in (4) the number of unknowns is three times larger than in (5). Indeed, the VIM uses all three components of the source and describes its effects onto the three components of the electric field at the observation point. In (5), the dipole distribution is oriented toward the normal components to the main lateral crack faces only [7]. This difference in the number of unknowns makes BEM largely faster than VIM for modeling of narrow crack response.

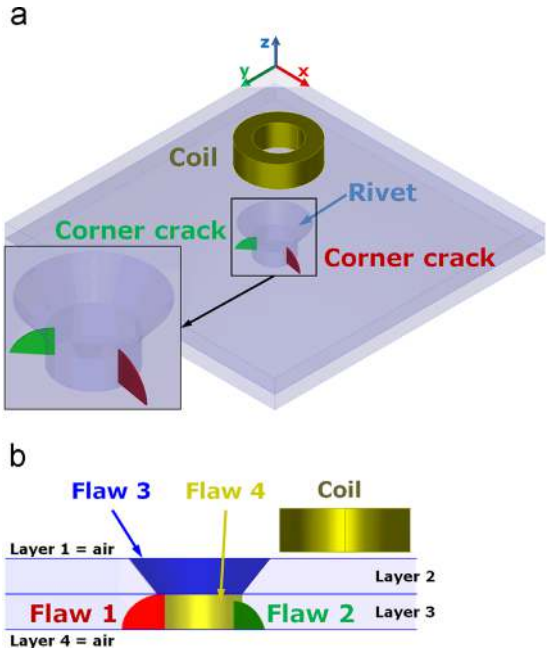

Fig. 1. Inspection of a fastener site inspection with an absolute pancake coil. (*a*) Two skewed corner cracks depart radially from the rivet and (*b*) detail of problem as it is considered from the electromagnetic modeling point of view.

From the pure numerical point of view, in the developed approach, we point out that in case of VIM the MoM employed is a Galerkin method based on pulsed basis-functions, whereas the BEM employs a MoM where pulse-basis and point-test functions are used. More details on analytical and numerical calculation of the DGF employed in (4) and (5) can be found in [9,1,2], respectively.

2.2. Coupled approach VIM–BEM

The theory introduced in the previous section is suitable to treat with good performance cases of volumetric flaws or narrow cracks, separately. Some applicative cases may involve, however, both volumetric objects and narrow cracks (see Fig. 1). To properly handle such problems we analyze it with respect to the "flaws characteristics", using a kind of *divide et impera* approach by considering each scattered object buried in the geometry either as volumetric flaw or as narrow crack.

Volumetric objects or narrow cracks crossing interfaces between layers are split, so that each object considered is present in one layer only and can thus be modeled by using Green dyads of its host layer. Then, a set of integral equations, describing all interactions between the fictitious dipole densities accounting for the flaws, is derived. These equations are either VIM ones if their self-term corresponds to a volumetric object, or BEM ones if their self-term corresponds to a narrow crack.

Let us consider now the problem sketched in Fig. 1. After applying the MoM [16], the strategy proposed above leads to the following matrix system of equations:

$$\begin{bmatrix} \mathrm{J}_1^{inc} \\ \mathrm{J}_2^{inc} \\ \mathbf{J}_3^{inc} \\ \mathbf{J}_4^{inc} \end{bmatrix} = \begin{bmatrix} 0 \\ 0 \\ \mathbf{p}_3 \\ \mathbf{p}_4 \end{bmatrix} - \begin{bmatrix} \mathrm{G}_{11}^{n_1 n_2} & \mathrm{G}_{12}^{n_1 n_2} & \underline{\mathbf{G}}_{13}^{n_1 3} & \underline{\mathbf{G}}_{14}^{n_1 4} \\ \mathrm{G}_{21}^{n_2 n_1} & \mathrm{G}_{22}^{n_2 n_2} & \underline{\mathbf{G}}_{23}^{n_2 3} & \underline{\mathbf{G}}_{24}^{n_2 4} \\ \underline{\mathbf{G}}_{31}^{3 n_1} & \underline{\mathbf{G}}_{32}^{3 n_2} & \underline{\mathbf{G}}_{33} & \underline{\mathbf{G}}_{34} \\ \underline{\mathbf{G}}_{31}^{3 n_1} & \underline{\mathbf{G}}_{42}^{4 n_2} & \underline{\mathbf{G}}_{\mathbf{43}} & \underline{\mathbf{G}}_{\mathbf{44}} \end{bmatrix} \begin{bmatrix} \mathrm{p}_1 \\ \mathrm{p}_2 \\ \mathbf{p}_3 \\ \mathbf{p}_4 \end{bmatrix}. \tag{6}$$

In (6), we can notice that the third and fourth rows correspond to the Fredholm equations of the second kind, whereas the first two rows correspond to the Fredholm equations of the first kind.

In (6) the vector sizes are $N_s \times 1$, with $s=1,2$, for J_1^{inc}, J_2^{inc} and p_1, p_2, whereas $\mathbf{J}_3$, $\mathbf{J}_4$ and $\mathbf{p}_3$, $\mathbf{p}_4$ have sizes of $3N_s \times 1$, with $s=3, 4$. The DGF, $\mathrm{G}_{11}^{n_1 n_1}$, $\mathrm{G}_{12}^{n_1 n_2}$, $\mathrm{G}_{22}^{n_2 n_2}$, $\mathrm{G}_{21}^{n_2 n_1}$ have sizes of $N_o \times N_s$, with $o, s=1, 2$. The Green dyads $\underline{\mathbf{G}}_{13}^{n_1 3}$, $\underline{\mathbf{G}}_{14}^{n_1 4}$, $\underline{\mathbf{G}}_{23}^{n_2 3}$ and $\underline{\mathbf{G}}_{24}^{n_2 4}$, in the matrix on the right-hand side have sizes $N_o \times 3N_s$ with $o=1$, 2 and $s=3$, 4, whereas the DGF $\underline{\mathbf{G}}_{31}^{3 n_1}$, $\underline{\mathbf{G}}_{41}^{4 n_1}$, $\underline{\mathbf{G}}_{32}^{3 n_2}$, $\underline{\mathbf{G}}_{42}^{4 n_2}$, have sizes $3N_o \times N_s$ with $o=3$, 4 and $s=1$, 2. N_o and N_s indicate the cells associated to the discretized observation and the source regions, respectively. The number of elements used to describe the volumetric flaws associated to the dyads $\underline{\mathbf{G}}_{34}$, $\underline{\mathbf{G}}_{43}$, $\underline{\mathbf{G}}_{33}$ and $\underline{\mathbf{G}}_{44}$ is $3N_o \times 3N_s$ with o, $s=3,4$, the number of elements being given by $N_i = N_{x_i} \times N_{y_i} \times N_{z_i}$ with $i=o, s$.

Let us focus our attention somewhat more on the DGF employed in the coupled approach and, in particular, on the elements that compose the dyadic matrix in (6). Inside this matrix, the diagonal blocks describe self-interactions of volumetric flaws and narrow cracks, respectively. The off-diagonal terms, however, correspond to interactions between different flaws, being narrow cracks or volumetric flaws. As previously said, we model the perturbation due to the presence of a narrow crack by describing the crack as a dipole distribution directed along the normal direction to the main lateral faces. This means that only normal components of the electric-dipole distribution act on the three components of the electric field at a point located inside the volumetric flaw. This description is an approximation, but differences in size between narrow cracks and volumetric flaws justify it make it from an engineering-like point of view. Indeed, the interaction between narrow cracks and volumetric flaws is weaker than the "main" interactions between narrow cracks and/or the self-interactions. In our experience, such a way to describe interactions between narrow cracks and volumetric flaw is enough to reach a good accuracy in the final result. One can imagine to avoid to keep into account these contributions by setting to zero the suitable off-diagonal terms inside the dyadic matrix in (6). Unfortunately, this choice may degrade, in certain cases, the accuracy in the final results.

3. Validation of coupled approach VIM–BEM

In order to validate the theoretical approach previously proposed, simulation results have been compared with precision experimental data [13]. Parameters of the ECT configurations considered are described in Table 1. These configurations have

Table 1
Benchmark data for a single layer and a multilayered structure: coil parameters, specimen and defect characteristics.

Plate 1		Hole 1	
Thickness	2.0 mm	Depth D_{H1}	2.0 mm
Conductivity	17.34 MS/m	Radius R_{H1}	10.0 mm
Plate 2		Hole 2	
Thickness	2.0 mm	Depth D_{H2}	2.0 mm
Conductivity	17.34 MS/m	Radius R_{H2}	10.0 mm
Dielectric insulator layer		Crack	
Thickness	0.07 mm	Depth D_{C2}	2.0 mm
		Length L_{C2}	9.8 mm
		Opening O_{C2}	0.234 mm
Coil			
Inner radius r_1			7.0 mm
Outer radius r_2			12.0 mm
Length l			4.0 mm
Number of turns N			1650
Lift-off lo			1.082 mm
Inductance (exp.) L_0			53.655 mH
Inductance (calc.) L_0			54.139 mH
Frequencies f			1.0, 5.0 kHz

been obtained from different assemblies of two plates, containing a hole or a hole and a narrow crack, respectively.

Concerning the numerical simulations performed, we have chosen to describe the holes with 35×5 and 35×8 elements along the diameter and the depth for frequency of 1 kHz and 5 kHz, respectively. The number of elements employed to describe the narrow crack with the BEM is five elements per skin depth for the crack depth and ten elements per coil outer radius for the crack length. To compare the performance of the coupled approach with the one of VIM only, a calculation with holes and crack modeled with VIM has also been run. In this particular case, the narrow crack is described with $30 \times 50 \times 8$ elements in terms of width, length and depth, respectively, at the frequency of 1 kHz.

The first problem involves an aluminum plate affected by a through-wall hole, from which departs radially a through-wall narrow crack (see Fig. 2(a)). The second one concerns a three-layered structure obtained by superposition of an aluminum plate affected by a through-wall hole and a crack, a very thin dielectric insulator and, as a third layer, another aluminum plate affected by a through-wall hole, identical to that of the first plate. The two holes are axially centered (see Fig. 2(b)). A pancake coil in absolute mode is used to inspect the structure for both problems.

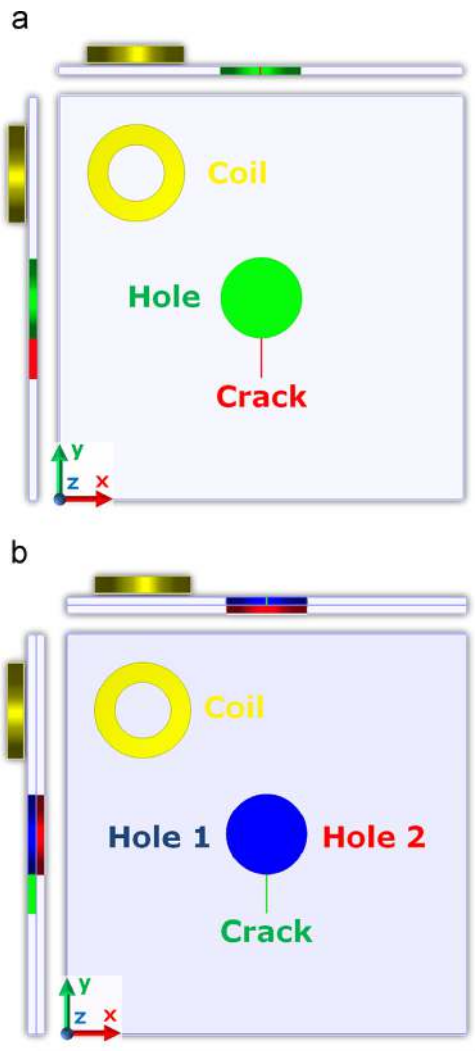

Fig. 2. Problems modeled to validate the VIM–BEM approach. In (a) the plate structure affected by a through-wall hole and a through-wall crack. In (b) the three-layered structure made by the stack the plate sketched in (a), a thin dielectric insulator and another plate affected with a through-wall hole. In both figures, views from the top and from the sides are presented.

Results obtained – without any calibration – for the single-plate case at a frequency of 1 kHz are plotted in Fig. 3. A very good agreement between the results obtained with the coupled approach VIM–BEM and the measurement is observed in the normalized complex plane (see Fig. 3(a)) when comparing normalized real and imaginary parts (see Fig. 3(b)) with respect to the coil scan along the crack line. As traditional, signals have been normalized with respect to the reactance of the coil in air (X_0). Besides, simulation results obtained with VIM only show a worse agreement with experimental data, compared to the VIM–BEM ones. This justifies the use of this coupled approach, treating accurately both narrow cracks and volumetric objects. From the computational point of view, the VIM–BEM takes about half the time compared to the VIM alone, which takes about 2 h and 30 min to compute a complete XY map made of 80×80 samples taken all around the flawed zones. The computer used for these simulations is an Intel-Q9550@2.83 GHz with 8 GB of RAM.

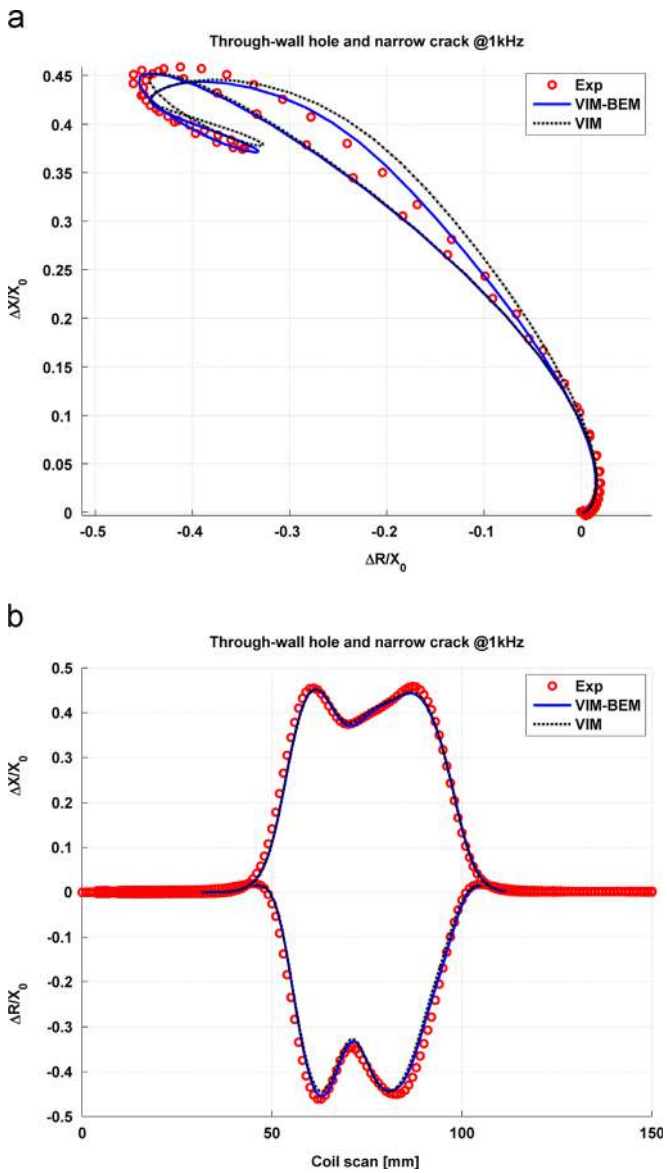

Fig. 3. Obtained results for the plate test case, with VIM–BEM (solid line), VIM (dotted) line and experimental data (circles). The variation of the real and imaginary parts is given in (a) in the normalized complex plane, and in (b) with respect to the coil motion. Both the results are normalized with respect to the reactance of the coil in air X_0.

In Fig. 4 we have displayed the results associated to the three-layered problem. ECT signals are plotted in the complex plane normalized with respect to the reactance of the coil in air (X_0) at the frequency of 1 kHz (see Fig. 4(a)) and at 5 kHz (see Fig. 4(b)). In both cases, the coupled approach is in very good agreement with the experiments. From the computational point of view, an increase in terms of simulation time appears, due to the presence of a second volumetric flaw (i.e. the second plate with the through-wall hole embedded in). The complete map, taken on 80×80 samples all around the flawed zones, has been performed at the frequency of 1 kHz, with the VIM–BEM model, in about 4 h and 40 min, whereas at 5 kHz the solution has been calculated in 4 h and 55 min. It is worth underlying that the computational effort claimed by the VIM alone in this second couple of problems does not allow to end-up with an accurate solution in acceptable time on our PC. In this way, we remark that the real bottleneck of the VIM–BEM approach is directly linked to the size of the problem, in terms of number of elements required to describe the volumetric flaw(s). Moreover, the presence of more than one narrow crack does not imply a dramatic increase in computational time. Due to these reasons, one can affirm that the coupled approach is very suitable to be applied in configurations where multiple narrow cracks appear in conjunction with "few" volumetric flaws. Finally, we note that the use of coarser grids for the volumetric objects allows to obtain in about 5 min the similar ECT signals, with a discrepancy versus experimental data smaller than 10%. Such performance in computational time cannot be obtained with VIM only, as the narrow cracks need to be very finely meshed with this method.

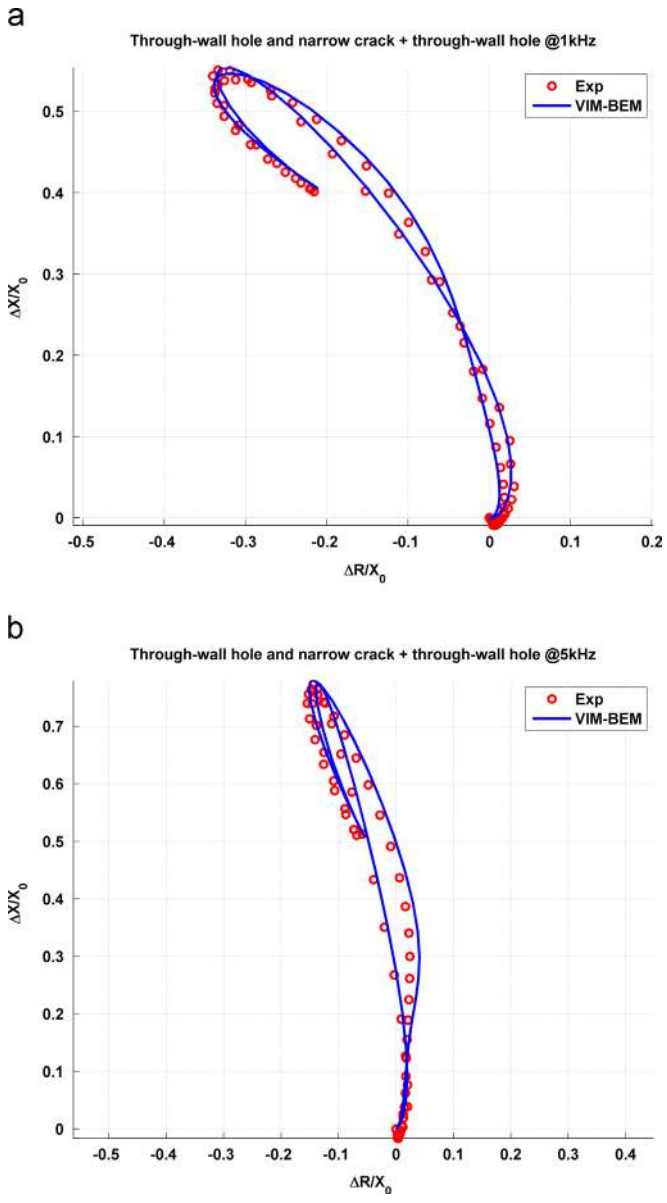

Fig. 4. Results obtained for the three-layered structure case, with VIM–BEM (solid line) and experimental data (circles) plotted in the complex plane normalized with respect to the reactance of the coil in air (X_0). In (a) the considered working frequency is 1 kHz and in (b) the working frequency is 5 kHz.

4. Comments and remarks on the VIM–BEM approach

The VIM–BEM approach presented in this paper aims to further extend the capability of both VIM and BEM beyond their native scope. Even though the possibility of treating a canonical geometry (either planar structure or cylindrical one, layered or homogeneous) may be seen as a limitation, we would like to mention that few restrictions concern the excitation source(s) considered in the proposed approach. Indeed, in very recent works the possibility of computing in fast and accurate way the incident field with different types of geometries and probes arrangements [15,17] greatly enlarges the application domain of the semi-analytical methods and thus the VIM–BEM also. More in general, by considering the semi-analytical approach here proposed and other coupling techniques, one should mention the paper [18,19]. In the first paper, the BEM model has been coupled with FEM in order to calculate the incident field due to complex sources (e.g. U-core probe and stick core probe) and the BEM has been employed to calculate the flaw response (e.g. rectangular slot) via a MoM approach. The second work proposes the calculation of the dyadic Green matrix elements by employing FEM, thus the linear system of equations associated to the MoM is solved in order to calculate the values of the unknown dipole distribution. The drawback of this second approach resides in the additional computational burden consisting in filling the dyadic Green function elements via the FEM. In the VIM–BEM approach, particular attention has been paid to the construction of the employed dyadic Green function and then to the suitable system of equations to solved in order to address, at the same stage, different kinds of flaws (i.e. volumetric objects and narrow cracks). In this way, considering the coupled [18], this approach can be employed straightforwardly in cases with complex excitation sources just by replacing the BEM model part with the presented VIM–BEM counterpart. It is worth also to mention that the coupling between FEM and VIM–BEM has the obvious payback of a low CPU time efficiency due to the FEM part.

5. Conclusions

In this paper, we have presented a novel approach based on a coupled use of VIM and BEM models. Theoretical developments have been validated with respect to precision laboratory-controlled measurements carried out on an academic configuration approximating the industrial application of rivet inspection. We have shown the accuracy and the reliability of the VIM–BEM approach in different test cases. Moreover, a non-negligible speed-up in terms of computational time has been achieved by employing the VIM–BEM approach instead of the VIM approach only. It has shown also that one may overcome the dramatic VIM limitation, in terms of computational effort, in the presented class of problems.

The speed-up in terms of performances and the overall good accuracy make the VIM–BEM approach a very interesting alternative to the complete VIM simulations for in problems involving both volumetric flaws and narrow cracks. Moreover, the VIM–BEM becomes even more powerful compared to the VIM, if the number of narrow cracks which affect the configuration studied increases. All the aforementioned points make the VIM–BEM approach the preferential choice, with respect to the standard VIM, in terms of forward problem solver to be employed in inversion algorithms. Indeed, as we have underlined in this paper, the computational cost of VIM may severely restrict the treatable problems in inversion procedure. Further extension of the proposed model could concern its use in the case of Pulsed Eddy Current Testing (PECT) following the so-called Frequency Domain Summation (FDS) approach, proposed recently by [20]. It worth underlying that in case of PECT signal simulation via FDS approach, the computational load required for the class of numerical problems may be, in certain case, not be negligible. Another interesting improvement would be the use of higher basis and testing functions like the Rao–Wilton–Glisson (RWG) [21]. This choice allows to describe in a more efficient and accurate way even more complex flaws regions. Finally, in the case of this particular application, the replacement of the planar dyadic Green operator by another one taking the hole into account [22] would suppress the VIM part, reducing the problem to a BEM one that would provide very accurate results within seconds.

Acknowledgments

This work has been performed within the CIVAMONT project framework which aims to collect collaboration of the academic world in developing modeling around the multi-method NDT software CIVA.

References

[1] Miorelli R, Reboud C, Lesselier D, Theodoulidis T. Eddy current modeling of narrow cracks in planar-layered metal structures. IEEE Trans Magn 2012;48:2551–9.
[2] Miorelli R, Reboud C, Theodoulidis T, Poulakis N, Lesselier D. Efficient modeling of ECT signals for realistic cracks in layered half-space. IEEE Trans Magn 2013;49:2886–92.
[3] Xiong JL, Chew SC. A newly developed formulation suitable for matrix manipulation of layered medium Green′s functions. IEEE Antennas Wirel Propag 2010;58:868–79.
[4] Chew WC, Chen SY. Response of a point source embedded in a Layered Medium. IEEE Antennas Wirel Propag Lett 2003;2:254–8.
[5] Chow YL, Yang JJ, Fang DG, Howard GE. A closed-form spatial Green′s function for the thick microstrip substrate. IEEE Trans Microw Theory Tech 1991;39:588–92.
[6] Hua Y, Sarkar TK. Matrix pencil method for estimating parameters of exponentially damped/undamped sinusoid in noise. IEEE Trans Acoust Signal Speech Process 1990;38:814–24.
[7] Bowler JR. Eddy-current interaction with an ideal crack. I. The forward problem. J Appl Phys 1994;75:8128–37.
[8] Bowler JR. Inversion of open cracks using eddy-current probe impedance measurements. In: Thompson DO, Chimenti DE, editors. Review of progress in quantitative nondestructive evaluation, vol. 15A. Plenum, New York: American Institute of Physics; 2000. p. 529–33.
[9] Reboud C, Pichenot G, Paillard S, Jenson F. Simulation and POD studies of riveted structures inspected using eddy current techniques. In: Knopp J, Blodgett M, Wincheski B, Bowler N, editors. Electromagnetic non-destructive evaluation (XIII), studies in applied electromagnetics and mechanics. Amsterdam: IOS Press; 2009. p. 129–36.
[10] Zeng Z, Yiming D, Xin L, Udpa L, Udpa SS, Koltenbah BEC, et al. C-GMR data analysis for inspection of multilayer airframe structures. IEEE Trans Magn 2011;47:4745–52.
[11] Theodoulidis T. Developments in efficiently modelling eddy current testing of narrow cracks. NDT&E Int 2010;43:591–8.
[12] Knopp JS, Aldrin JC, Jata KJ. Computational methods in eddy current crack detection at fastener sites in multi-layer structures. Nondestruct Test Eval 2009;24:103–20.
[13] Martinos J, Theodoulidis T, Poulakis N, Tamburrino A. A benchmark problem for eddy current nondestructive evaluation. IEEE Trans Magn, http://dx.doi.org/10.1109/TMAG.2013.2282259, in press.
[14] Auld BA, Muennemann FG, Riaziat M. Nondestructive testing, chapter 2, quantitative modelling of flaw responses in eddy current testing. London: Academic Press; 1984.
[15] Reboud C, Theodoulidis T. Field computations of inductive sensor with various shapes for semi-analytical ECT simulation. In: Rao BPC, Jayakumar T, Balasubramanian K, Raj B, editors. Electromagnetic non-destructive evaluation (XV), studies in applied electromagnetics and mechanics. Amsterdam: IOS Press; 2012. p. 3–10.
[16] Harrington RF. Field computation by moment methods. New York: MacMillan; 1983 Florida: Krieger Publishing.
[17] Skarlatos A, Demaldent E, Vigneron A, Reboud C. Modelling of specimen interaction with ferrite cored coils by coupling semi-analytical and numerical techniques. To be published in electromagnetic non-destructive evaluation (XVII), studies in applied electromagnetics and mechanics, Amsterdam: IOS Press; 2014.
[18] Le Bihan Y, Pávó J, Bensetti M, Marchand C. Computational environment for the fast calculation of ECT probe signal by field decomposition. IEEE Trans Magn 2006;42:1411–4.
[19] Badics Z, Pávó J, Komatsu H, Kojima S, Matsumoto Y, Aoki K. Fast flaw reconstruction from 3D eddy current data. IEEE Trans Magn 1998;34:2823–8.
[20] Theodoulidis T, Wang H, Tian GY. Extension of a model for eddy current inspection of cracks to pulsed excitations. NDT&E Int 2012;47:144–9.
[21] Rao SM, Wilton DR, Glisson AW. Electromagnetic scattering by surfaces of arbitrary shape. IEEE Trans Antennas Propag 1982;30:409–18.
[22] Skarlatos A, Theodoulidis T. Solution to the eddy-current induction problem in a conducting half-space with a vertical cylindrical borehole. In: Proceedings of the Royal Society A; 2012. rspa.2011.0684v1-rspa20110684.